

On the metal abundances inside mixed-morphology supernova remnants: the case of IC443 and G166.0+4.3

F. Bocchino(1) M. Miceli(2) E. Troja(3,4)

1 - INAF-Osservatorio Astronomico di Palermo, Piazza del Parlamento 1, 90134 Palermo, Italy

2 - Consorzio COMETA, Via S. Sofia 64, 95123 Catania, Italy

3 - INAF - Istituto di Astrofisica Spaziale e Fisica Cosmica, Sezione di Palermo, via Ugo la Malfa 153, 90146 Palermo

Abstract

Recent developments on the study of mixed morphology supernova remnants (MMSNRs) have revealed the presence of metal rich X-ray emitting plasma inside a fraction of these remnant, a feature not properly addressed by traditional models for these objects. Radial profiles of thermodynamical and chemical parameters are needed for a fruitful comparison of data and model of MMSNRs, but these are available only in a few cases. We analyze XMM-Newton data of two MMSNRs, namely IC443 and G166.0+4.3, previously known to have solar metal abundances, and we perform spatially resolved spectral analysis of the X-ray emission. We detected enhanced abundances of Ne, Mg and Si in the hard X-ray bright peak in the north of IC443, and of S in the outer regions of G166.0+4.3. The metal abundances are not distributed uniformly in both remnants. The evaporating clouds model and the radiative SNR model fail to reproduce consistently all the observational results. We suggest that further deep X-ray observations of MMSNRs may reveal more metal rich objects. More detailed models which include ISM-ejecta mixing are needed to explain the nature of this growing subclass of MMSNRs.

1 Introduction

Mixed-morphology supernova remnants (MMSNRs) have been traditionally defined as remnant having a shell morphology in radio and a centrally peaked morphology in the X-ray band characterized by a thermal spectrum (Rho & Petre 1998). The origin of this atypical morphology is controversial. Traditional models mostly relies on the effects of thermal conduction (e.g. Cox et al. 1999, Shelton et al. 1999, White & Long 1991), but there are also models which invoke projection effects (Petruk

2001). Tilley et al. (2006) tried to refine previous analytical models by using a set of hydrodynamical simulations aimed at reproducing the morphology observed in MMSNRs.

In parallel to these theoretical efforts, there is a growing observational interest around MMSNRs, which has led in a few cases to useful comparison with models. Slane et al. (2002) favor the evaporating clouds White & Long (1991) model for G290.1-0.8 (rather than the radiative model of Shelton et al. 1999), but problems remain in the comparison of the surface brightness profiles. Lazendic & Slane (2006) also find a reasonable agreement between both models and X-ray observations of CTB1 and HB21, but they point out that the predicted central density are below the derived densities of the emitting plasma. Rho & Borkowski (2002), instead, argue that the White & Long (1991) evaporating cloud model is at odds with the presence of a strong radiative shock front in the MMSNR W28, but also the radiative model is at odd with the strong thermal variation found in this remnant (see also Chevalier 1999 for a critical approach to the evaporating cloud model of MMSNRs).

In addition, several authors have pointed out that part of the X-ray emission of MMSNRs may be composed by thermal plasma with high metal abundances, as those observed in stellar ejecta inside young historical SNRs (e.g. Shelton et al. 2004, Chen et al. 2008), or in other Galactic (e.g. Vela SNR, Miceli et al. 2008; Cygnus Loop, Katsuda et al. 2008; Puppis A, Hwang et al. 2008) and Magellanic Cloud SNRs (e.g. 0103-72.6, Park et al. 2003a; N49B, Park et al. 2003b). This important result was addressed and summarized by Lazendic & Slane (2006), which report a compilation of 26 MMSNRs, 10 of which show some sign of enhanced metal abundances in the X-ray spectrum. It is important to stress at this point that the presence of enhanced metal abundances inside MMSNRs has not been addressed in detail yet in the models developed for this sub-class of remnants. In general, published models with thermal conduction do not take into account the mixing of ejecta with the circumstellar and interstellar medium, so the emerging class of metal rich MMSNRs is still not properly understood. This is also the reason why the comparison between models and observation has mostly focused only on morphological issues, with the general comment that the presence of the additional ejecta component may reconcile the discrepancy between model and observed profile (like in the case of W44, Shelton et al. 2004).

The mixed morphology category of SNRs (and especially the emerging subclass of metal-rich MMSNRs) can be better understood if we have a large sample of objects with well studied characteristics. In particular, the accurate determination of density, temperature and abundances profile for MMSNRs will allow us to perform an accurate comparison with both traditional ISM models and a new magnetohydrodynamical (MHD) model of shocked ISM and ejecta inside MMSNRs, subject to a forthcoming publication.

We have undertaken a systematic review of the MMSNRs listed in Lazendic & Slane (2006) with the primary goal to measure the abundances in the inner region of the remnants and other X-ray properties. In this paper, we review the XMM-Newton archive observations of two bright MMSNRs, IC443 and G166.0+4.3, with the aim of deriving the

distribution of temperature and metal abundances inside these remnants. Both our targets are mentioned in the list of Lazendic & Slane (2006) as MMSNRs with standard metal abundances. However, Troja et al. (2006) and Troja et al. (2008) have studied in detail the X-ray emission of IC443, and they have found enhanced metal abundances in a remarkable ring feature around the pulsar wind nebula, in the southern part of the remnant, attributed to emission from shocked ejecta. The compilation of MMSNRs with enhanced metal abundances needs therefore to be updated with new results from deep X-ray observations of MMSNRs. On the light of these new observational results, traditional models should be further verified and revised as necessary.

The paper is organized as follows: in Sect. 2 and 3 we present the results obtained from XMM-Newton archive observations of IC443 and G166.0+4.3, respectively. In Sect. 4, we present the comparison of our results with the standard models for MMSNRs, namely the evaporating clouds White & Long (1991) model and the radiative SNR model of Cox et al. (1999). In Sect. 5, we present the conclusion of our work.

2 IC443

IC443 has been observed in several bands and extensively studied in the literature and, for this reason, it is a case study for the interaction between SNR shocks and molecular clouds. Recent X-ray studies includes Troja et al. (2008), Bykov et al. (2008), Troja et al. (2006), while for infrared and radio studies see Noriega-Crespo et al. (2008), Bykov et al. (2008), Lee et al. (2008), Rosado et al. (2007), Leahy (2004) and references therein. The remnant has been classified as mixed-morphology by Rho & Petre (1998), based on observations with the ROSAT satellite. Troja et al. (2006) and Troja et al. (2008) confirm the centrally peaked morphology between 0.5 and 5 keV, with a bright X-ray peak near $06^h 17^m 09^s + 22^\circ 45^m$ in the 1.4–5 keV (Fig. 1). However, they note that, at very soft energies (0.3–0.5 keV), the remnant shows an incomplete shell extending from N to E, corresponding to one of the region of interaction with a large cloud. They have also investigated the spatial distribution of the metals inside this remnant, using the technique of the equivalent width images. According to them, the distribution of Si and S is far from being homogeneous. In particular, a ring of metal rich plasma surrounding the pulsar wind nebula is evident in the equivalent width images of these two elements (see their Fig. 3). Moreover, the northern region of the remnant, coincident with the maximum of the hard X-ray image (Fig. 1), is also characterized by a large value of the Si and S equivalent width, suggesting higher metal abundances with respect to surrounding regions. In the following, we focus on this region.

The data we use in this work are part Calibration and Performance Verification phase of the *XMM-Newton* satellite (Jansen et al. 2001), for a total of 6 observations of IC443. In addition, we have used the public archive observation 0301960101. The datasets we have used are the same datasets used by Troja et al. (2008). We screened both PN and MOS data using the algorithm suggested by Snowden & Kuntz (2007).

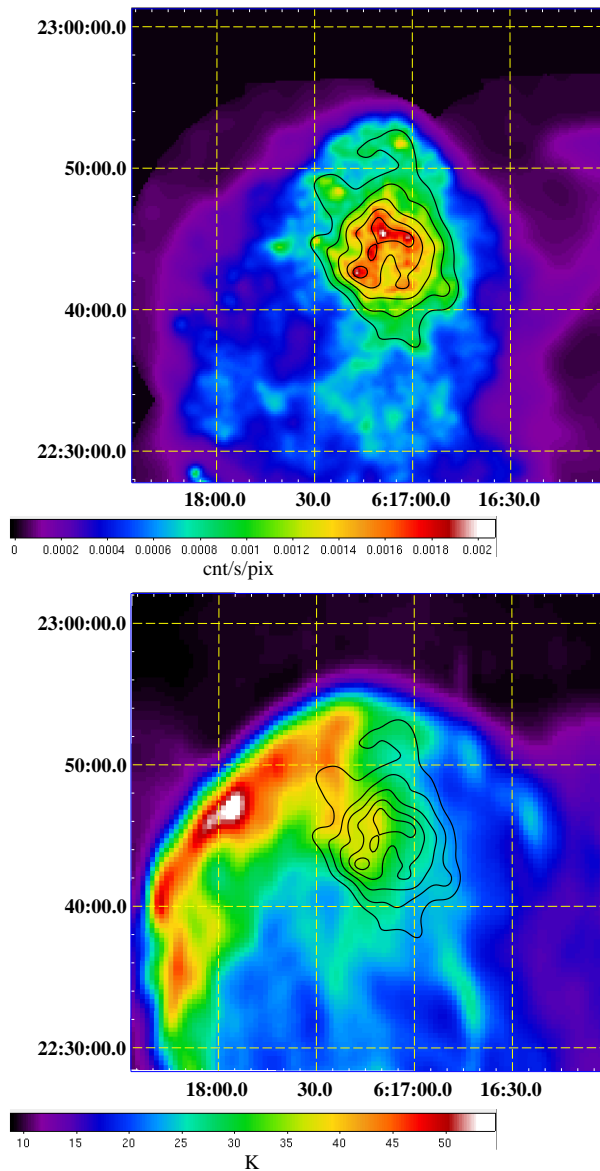


Figure 1: *Top*: XMM-Newton EPC mosaic of the northern region of the IC443 supernova remnant in the 1.4–5.0 keV band. The image is background subtracted and vignetting corrected. The pixel size is 10 arcsec. Five contours levels at $8, 10, 12, 14$ and 16×10^{-4} $\text{cnt s}^{-1} \text{pix}^{-1}$ are overlaid. These contours have been used as boundaries for the 5 spectral extraction regions discussed in the text. *Bottom*: same region at 1420 MHz (total intensity map) with X-ray contours overlaid (adapted from Leahy 2004).

The results are reported in Fig. 3. In order to study the profile of the thermodynamical and chemical parameters of this remnant, we have chosen 5 spectral regions defined in terms of contours of iso-surface brightness, centered in the bright northern region, as shown in Fig. 1. For each region, we have computed a mean distance from the X-ray peak as the average of the distance of all the pixel in that region. XMM-Newton PN and MOS spectra have been extracted using the software SAS 7.1 and corrected for detector non-uniformity using the task *evigweight*. Troja et al. (2006) have shown that the X-ray emission in the IC443 interior is composed by two thermal components, the soft one with temperature in the range 0.3–0.7 keV, in non-equilibrium of Ionization (NEI), and the second one with $kT = 1.1 - 1.8$ keV, in equilibrium of ionization (CIE). The soft component has been associated with the shocked interstellar material, while the hot component to the shocked stellar ejecta. Therefore, we have used the same emission models, namely the MEKAL model (Mewe et al. 1985) and the VNEI (Borkowski et al. 2001) model of XSPEC v11.3.2 (Arnaud 1996). We have fixed the chemical abundances of the soft component to solar values, and left the abundances of the hot component free to vary. The adopted models represent an approximation of the true conditions inside this complex remnant. However, this approach allows us to measure quantitatively the emission measure weighted temperature and metal abundances for each component in each spectrum. Moreover, by using the region layout shown in Fig. 1, we may derive meaningful constrain to any trend of the measured quantities related to the radial distance of the regions.

In Fig. 2, we show an example of spectrum, while the complete results of the spectral analysis are reported in Fig. 3 for the 5 spectral regions, displayed in order of increasing distance from the putative center. The temperature does not show large variations, indicating that thermal conduction must be efficient. The innermost regions are characterized by a higher metal abundances for Ne, Mg and Si. In these cases, the profiles show a decreasing trend with increasing distance from the center. While Ne and Mg retain over-solar of abundances in most regions, Si is above 1 only in the two innermost regions. On the other hand, S and Fe seems to have more uniform abundances, about 1.0 and 0.3 respectively. The thermodynamical parameters of both the components are in general agreement with the findings of Troja et al. (2006). The abundances patterns are generally consistent with the ones found by Troja et al. (2008) in the south region of the remnant, but smaller in value if compared to the remarkable ejecta ring surrounding the pulsar wind nebula found by them. Troja et al. (2008) have also compared the Mg/Si, S/Si and Fe/Si ratios of the ring with the nucleosynthesis model of core-collapse (Woosley & Weaver 1995) and Type Ia (Badenes et al. 2003) supernovae, finding more agreement with the former. We have verified that Mg/Si, S/Si and Fe/Si ratios found by us in the innermost spectral region in Fig. 1 are in agreement with those of the ring region, thus we concluded that our results also support a Type II progenitor for IC443.

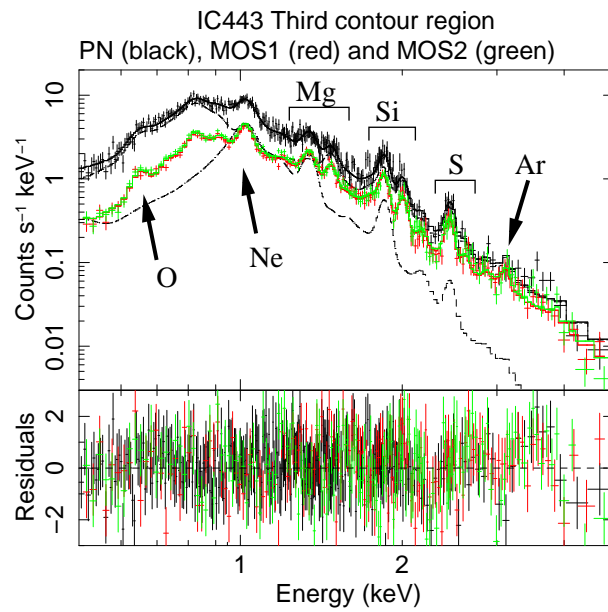


Figure 2: XMM-Newton EPIC spectrum of the third contour region in Fig. 1 (average distance $2.8'$ in Fig. 3). The best fit two thermal component model is shown as continuous line (with residual in lower panel), while individual components are shown in dashed black lines for the PN spectrum only. Emission lines from O (0.6–0.8 keV), Ne (~ 1 keV), Mg (~ 1.4 keV), Si (1.8–2 keV), S (~ 2.5 keV) and Ar (~ 3 keV) are visible.

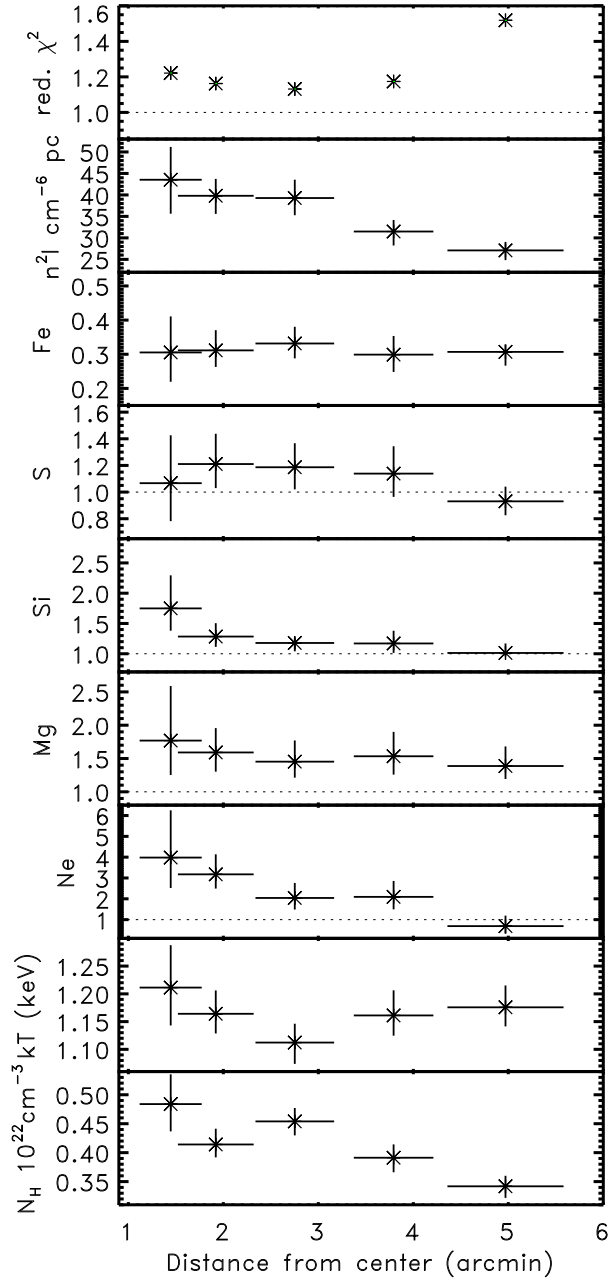


Figure 3: Results of the spectral fittings to the hard thermal component obtained in the 5 iso-brightness regions in IC443. See Fig. 1 for the position of the contours levels used for the region definition. Abundances are relative to solar values. The abscissa contains the average distance from the center (horizontal error bars are standard deviations). Vertical error bars are 2σ uncertainties. The normalization of the spectrum is expressed in terms of n^2l , where n is the plasma density and l is its extension along the line of sight.

3 G166.0+4.3 (VRO 42.05.01)

G166.0+4.3 is a supernova remnant in the anti-center direction whose X-ray and radio morphology has drawn considerable interest in the literature. Burrows & Guo (1994) and Guo & Burrows (1997) have reported on the ROSAT and ASCA X-ray observations of this remnant, finding a centrally peaked morphology which seems to be totally enclosed within the radio emission of this object. The latter, in turn, has a limb brightened double shell morphology, with a small diameter half-shell at NE (about 30', a.k.a. the shell) and a larger incomplete shell at SW (a.k.a. the wing, Pineault et al. 1985, Pineault et al. 1987, Leahy & Tian 2005 and references therein).

G166.0+4.3 was observed by *XMM-Newton* on 21 February 2003 (ID 0145500101) and on 23 February 2003 (ID 0145500201). The first observation was pointed at the western part of the remnant (the “wing”), for a total PN exposure after the screening procedure of 5.0 ks, while the second one was pointed to the small incomplete shell at the east. This latter pointing was severely contaminated by high energy proton flares and the net PN exposure time is only 1 ks, and we have not used it for spectral analysis.

A mosaic map of this remnant in the band 0.3–5.0 keV, obtained using the two *XMM-Newton* archive observations, is shown in Figure 4, which also include the 1420 MHz radio map of the Canadian Galactic Plane Survey (Taylor et al. 2003). The X-ray morphology derived by previous observations is confirmed, and the bright region (named “western bright knot” by Burrows & Guo 1994) is resolved for the first time, showing an elongation in the NW-SE direction. On the light of its radio and X-ray morphology, this remnant may be considered part of the sub-class of mixed-morphology (MM) SNRs introduced by Rho & Petre (1998). The adopted explanation of the peculiar radio morphology dates back to Pineault et al. (1987) and involves the explosion in a moderately dense medium followed by the breaking out of the shock in a rarefied hot tunnel, followed in turn by the interaction with again a denser medium. Guo & Burrows (1997) have made the only measurements of metal abundances in the X-ray spectrum of G166.0+4.3, finding a substantial underabundance of Mg, Si and Fe in the western bright knot and in the SE and NE of the wing.

In order to study the abundances in the centrally peaked region of G166.0+4.3, we tried to characterize the thermal properties in the plasma of this remnant by selecting 4 interesting regions for spectral analysis, which are shown in Fig. 4. Regions 1,2 and 3 are similar to region 1, 2 and 3 of Guo & Burrows (1997), but they are considerably smaller and pointed to bright features, and therefore they are much less affected by background (also considering the smaller *XMM-Newton* PSF compared to the ASCA one). In each region, we fitted the X-ray spectra with a Mewe et al. (1985) spectral model modified by interstellar absorption and letting the abundances of O, Ne, Mg, Si, S and Fe free to vary. In Fig. 5, we show, as an example, the spectrum of region 1. The results of the spectral analysis are presented in Fig. 6, and indicate low variation of temperature (up to 10%) and large variation of interstellar absorption

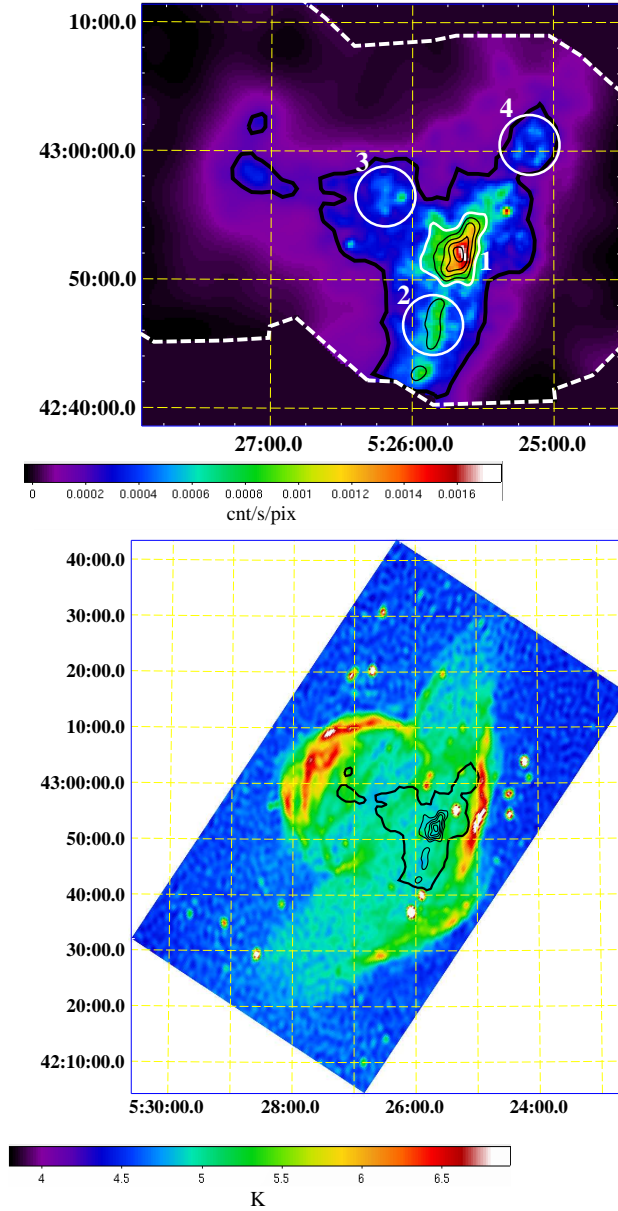


Figure 4: *Top*: *XMM-Newton* EPIC images of G166.0+4.3 in the 0.3–5 keV background subtracted and vignetting corrected. Black thick contour is at $0.2 \times 10^{-3} \text{ cnt s}^{-1} \text{ pix}^{-1}$ and black thin contours correspond to 0.6, 0.8, 1.0, 1.2 and $1.5 \times 10^{-3} \text{ cnt s}^{-1} \text{ pix}^{-1}$ (1 pixel = $12'' \times 12''$). Numbers mark the spectral extraction region used in the text (Region 1 is defined by the outermost thin surface brightness contour). The *XMM-Newton* EPIC field of view is marked in white (two observations combined). *Bottom* 1420 MHz CGPS DRAO radio image of G166.0+4.3 (adapted from Leahy & Tian 2005). X-ray contours of the top panel are shown in black.

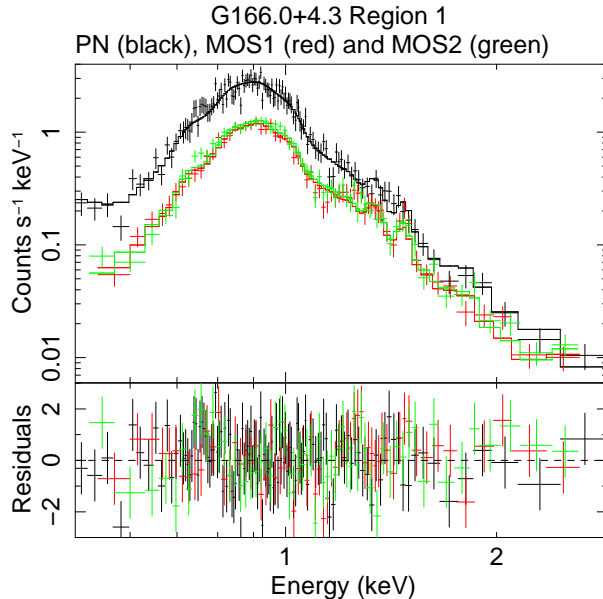


Figure 5: XMM-Newton EPIC spectrum of the G166.0+4.3 Region 1 in Fig. 4. The best fit thermal model is shown as continuous line (with residual in lower panel).

(up to 50%). The variation patterns seems to be more in agreement with those found by Burrows & Guo (1994) than those of Guo & Burrows (1997). The regions seems to be characterized by an underabundance of O and Si and an overabundance of S, while Ne, Mg and Fe seems to be around solar values. Our Mg, Si and Fe abundances are in agreement with Guo & Burrows (1997), who also found a value of $\lesssim 1$ for the abundances of these elements. A thermal model in Non-Equilibrium of Ionization do not improve the fits in the regions, giving a ionization time $\tau \gtrsim 10^{12}$ s cm^{-3} and abundances very similar to the one we obtained with the equilibrium model.

We have investigated if there is a radial gradient of metal abundances variations inside the bright region 1 of the remnant (the “western bright knot”), in a manner similar to what we have done in Sect. 2 for IC443, but, given the low counting statistics, the results are not constraining.

4 Discussion

IC443 and G166.0+4.3 were listed in the Lazendic & Slane (2006) work as standard abundances MMSNRs. However, the spatially resolved spectral analysis we have done on the bright X-ray central regions of IC443 has pointed out that this object belong to the subclass of metal rich mixed morphology remnant. In the case of G166.0+4.3 there is no compelling

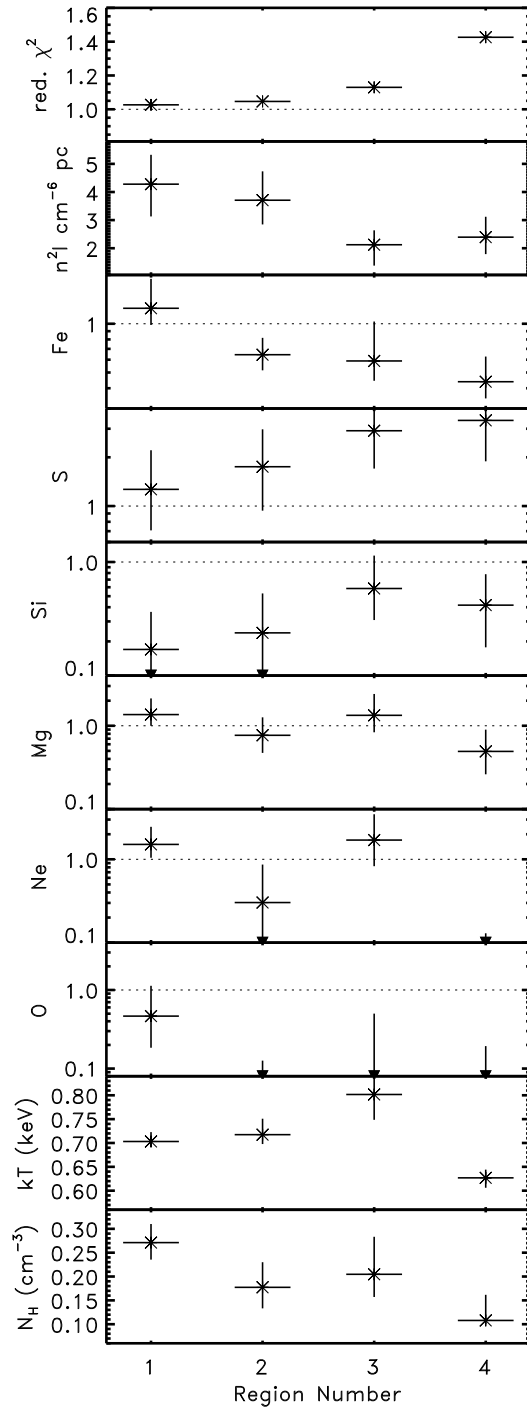


Figure 6: Spectral fitting results of regions 1–4 in G166.0+4.3. See Fig. 4 for the position of the regions. Black arrows indicates a lower limit of 0.

evidence for enhanced metal abundances apart from sulfur in the outer regions. The short exposure time of the XMM-Newton observation of the latter has prevented us to study possible trends of metal abundances in the core of this remnant. Our results suggest that it is important to review the list of MMSNRs of Lazendic & Slane (2006) to properly address the issue of the chemical abundances in all the known remnant of this kind. Other MMSNRs may be erroneously cataloged as standard abundances objects.

It is not straightforward to understand if the high metal abundances seen in some of the MMSNRs is a general property, or if represent just an evolutionary phase of the life of these objects, or it depends on the initial remnant composition. From the theoretical point of view, the evaporating cloud model of White & Long (1991) and the radiative SNR model Cox et al. (1999), traditionally used to explain the centrally peaked thermal X-ray morphologies, can be of limited help in understanding the subclass of the metal rich MMSNRs, since they do not consider in detail the mixing between ejecta and shocked material inside the remnants. However, these model have been often used to interpret the X-ray emission of some MMSNRs (e.g. Bocchino & Bandiera 2003, Lazendic & Slane 2006), so it is worth to perform a detailed comparison with our results to underline their limitations and to drive the exploration of new ones.

We first consider the evaporating cloud model of White & Long (1991), in which the X-ray central enhancement is due to the material ablated by shock heated clouds inside the remnant. The models depends on the traditional E (the explosion energy), ρ (the preshock ISM density), t (the age of the remnant) plus two parameters describing the evaporating clouds, namely C (the ratio of mass in clouds to mass in the intercloud medium) and τ (the ratio of the cloud evaporation time scale to the SNR age). With an appropriate choice of normalized quantities for the radial profiles (for what concern our study, we will consider the density normalized to the post-shock density, ρ/ρ_s , the temperature normalized to the shell temperature T/T_s , and the normalized emission measure $EM(\pi R_s^2)/EM(tot)$ see their Figure 4), they show that the dependence on E , ρ_0 and t can be masked out in the presentation of the results. To ease the comparison with observations, the authors discuss the asymptotic behavior of their model when C and $\tau \rightarrow \infty$, in which case the model only depend on the ratio C/τ . In Fig. 7, we show the normalized temperature, density and emission measure for the models with $C/\tau = 0, 1, 2, 3$ and 4 . To further ease the comparison with the data, we decided to normalize the temperature and density to their respective central values, instead of their shell values, like in the work of White & Long (1991). In fact, in our observations (and in general in all the MMSNR observations) the low X-ray surface brightness at the shell prevents an accurate spectral analysis, so it is particularly difficult to estimate the shell values. On the other hand, the central regions are by definition the brightest, and we may get more accurate results. One more point of concern in the comparison between models and our two targets is the value of the shell radius, used to normalize the abscissa of the profiles and the emission measure. IC443 and G166.0+4.3 have far from circular symmetric morphologies and offset X-ray peaks, so it is particular difficult to estimate a single shell radius.

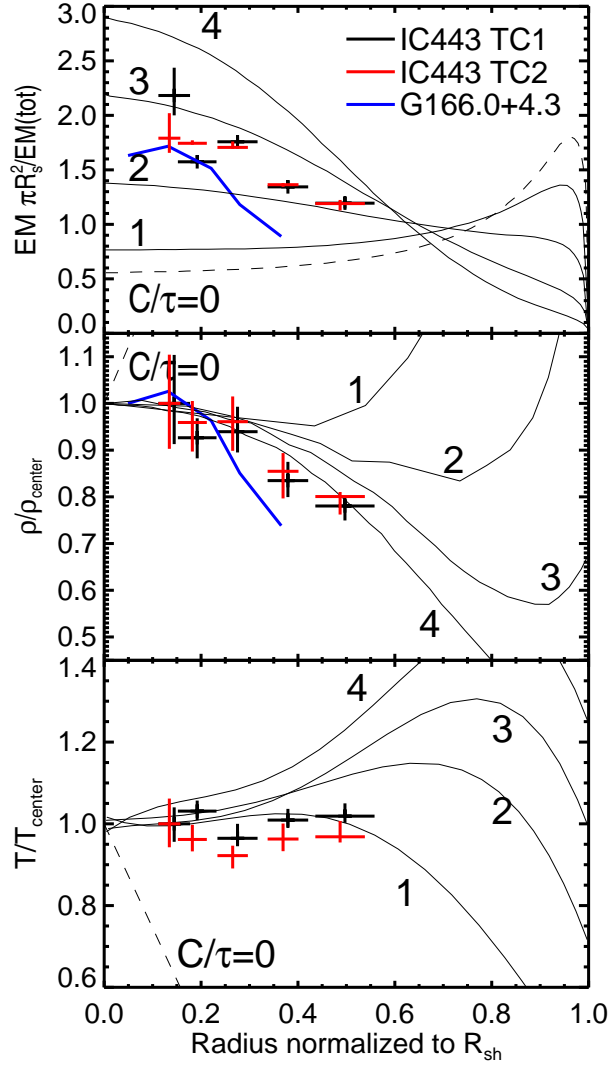


Figure 7: Comparison between the White & Long (1991) evaporating cloud model and the observed profiles in IC443 and G166.0+4.3. *Top*: Normalized emission measure (see text for explanation). *Middle*: Density normalized to central value. *Bottom*: post-shock temperature normalized to central value. Black and red crosses are IC443 low and high temperature component data with uncertainties, respectively; blue curves are G166.0+4.3 data. Black curves are White & Long (1991) profiles for models with $C/\tau = 0$ (dashed), 1, 2, 3 and 4. The distance from the center is normalized to the shell radius (assumed $10'$ for IC443 and $\sim 6.5'$ for G166.0+4.3, see text for details).

For IC443, we have used a radius of $10'$ (~ 4.3 pc at 1.5 kpc distance), because it is the average distance of the radio shell from the X-ray peak in the East, North and West of the remnant. For G166.0+4.3, we have used $\sim 6.5'$ (~ 13 pc at 4.5 kpc distance), which is the distance to the east radio wing.

In Fig. 7, we also plot the derived values for the low and high temperature component of IC443 and for the single thermal component of G166.0+4.3. The profiles of G166.0+4.3 seems to be steeper than the profiles of IC443. In general, a reasonably good agreement can be found between the observed normalized emission measure and the model with $C/\tau = 2 - 3$ for both objects, even if the uncertainties about the adopted shell radius may affect the actual result. However, it is important to stress that the density and temperature profiles are not entirely consistent with the emission measure profiles. In case of IC443, the density profile would be more in agreement with $C/\tau \geq 4$, while the temperature profile with $C/\tau < 1$. It is worth noting that the inconsistency is present in both the thermal components of IC443, and that it also holds for the density of G166.0+4.3 which would indicate $C/\tau > 4$. Conversely, we could use the density profile to find a good fit to the model by varying the shell radius within a $\pm 50\%$ range, but the emission measure and temperature profile would be still inconsistent. For instance, we have verified that the emission measure would be much more centrally peaked than observed. Finally, we note that the central peak in both the observed density profiles seems to exclude evaporating cloud models with low values of τ (cfr. Fig. 1 in White & Long 1991).

In summary, the comparison with the evaporating cloud model points toward high values of τ , but cannot be considered very informative on the actual value of C and τ , and indicates that the observed density profiles are usually steeper than what predicted by the model which best fit the emission measure profiles, a situation which cannot be explained in terms of an ejecta component in addition to the evaporating cloud component. In the latter case, in fact, we would expect the density profile be shallower than the model, because of the additional density provided by the ejecta. We therefore conclude that the X-ray morphology of these remnants is not compatible with the evaporating cloud model. The temperature profiles, though not entirely consistent with the model, seems to indicate in any case very limited variations, and therefore points toward efficient thermal conduction inside both the remnants. The failure of the cloud evaporation model and the high efficiency of the thermal conduction suggest an explanation in terms of the entropy-mixed thermally conductive model suggested by Shelton et al. (2004) to explain the MMSNR W44, possibly amended to take into account the peculiar environment in which these remnants are expanding. A detailed numerical model of the metal rich MMSNRs taking into account the mixing between ejecta and shocked ISM material, the thermal conduction and a realistic model for the environment, is required to verify this scenario.

The comparison with the radiative model of Cox et al. (1999) can be done more straightforwardly following Lazendic & Slane (2006) assuming that the actual shock radius is the radius at which the remnant enters the radiative stage. This yields a lower limit of the ambient and central densi-

ties, following the relations of Cox et al. (1999). Using realistic radius values, as the one we have used in the comparison with the cloudy ISM model, we get ambient density lower limits of the order of 10 cm^{-3} . While it is true that in both the remnants there is substantial evidence of expansion in dense environments, it is also true that it is very unlikely that the expansion occurred *always* in a medium so dense. For IC443, Troja et al. (2006) argued that the remnant evolved inside wind blown bubble, an hypothesis originally suggested by Braun & Strom (1986), while for G166.0+4.3, Gaensler (1998) argued the remnant has expanded in a low density hot tunnel before to encounter recently a high density region. The hot tunnel putative location is right where the X-ray emission peak is located. In both cases, therefore, it is very unlikely that a radiative model which assumes a long evolution inside a very dense medium is applicable, as it is whenever there is evidence of a massive progenitor star, which usually have strong pre-supernova winds. Chen et al. (2008) suggest that the X-ray emission of Kes 27 MMSNR may be explained in term of a shock reflected by a cavity wall, a mechanism which may be at work also in IC443 and G166.0+4.3, given the evidences on their environments.

5 Summary and conclusion

We report on XMM-Newton X-ray observation of the two supernova remnant IC443 and G166.0+4.3, with particular emphasis on the nature of their centrally peaked thermal X-ray emission above 1 keV. We confirm that the X-ray morphology of these remnants entitle them to be included in the class of mixed morphology SNRs. Contrary to what was previously known, we find that the chemical abundances of the bright central peak of IC443 are above solar, promoting this object in the recently pointed out subclass of metal rich MMSNRs. For G166.0+4.3, there is no evidence of enhanced metal abundances, except maybe for sulfur in the outer regions, but the limited quality of the data prevented us to perform spatially resolved spectroscopy of the central peak.

We derived profiles of metallicity, temperature, density and emission measure, and we compared them with prediction of the White & Long (1991) and Cox et al. (1999) models, traditionally used to explain the MMSNR morphology in other objects. We have found that the observed profiles are inconsistent with the models, and we argue that a more detailed modeling including the mixing of ISM and ejecta material is required to explain the observations. The entropy mixing model of Shelton et al. (2004) seems to be the most promising starting point for a more detailed modeling, though the effects of the complex environment in which the MMSNRs seems to be located (Lazendic & Slane 2006) and the projection effects as discussed by Petruk (2001) should be taken into account. Temperatures, density, and chemical abundances profiles of MMSNRs are therefore the key observational constraints to compare with future models.

We thank D. Leahy for providing us with the 1420 MHz total intensity map of IC443 in electronic format. We also thank O. Petruk and S. Orlando for useful comments on this work. This work makes

use of results produced by the PI2S2 Project managed by the Consorzio COMETA, a project co-funded by the Italian Ministry of University and Research (MIUR) within the Piano Operativo Nazionale “Ricerca Scientifica, Sviluppo Tecnologico, Alta Formazione” (PON 2000-2006). More information is available at <http://www.consorzio-cometa.it>.

References

- Arnaud, K. A. 1996, in *Astronomical Society of the Pacific Conference Series*, Vol. 101, *Astronomical Data Analysis Software and Systems V*, ed. G. H. Jacoby & J. Barnes, 17–+
- Badenes, C., Bravo, E., Borkowski, K. J., & Domínguez, I. 2003, *ApJ*, 593, 358
- Bocchino, F. & Bandiera, R. 2003, *A&A*, 398, 195
- Borkowski, K. J., Lyerly, W. J., & Reynolds, S. P. 2001, *ApJ*, 548, 820
- Braun, R. & Strom, R. G. 1986, *A&A*, 164, 193
- Burrows, D. N. & Guo, Z. 1994, *ApJL*, 421, L19
- Bykov, A. M., Krassilchtchikov, A. M., Uvarov, Y. A., et al. 2008, *ApJ*, 676, 1050
- Chen, Y., Seward, F. D., Sun, M., & Li, J.-t. 2008, *ApJ*, 676, 1040
- Chevalier, R. A. 1999, *ApJ*, 511, 798
- Cox, D. P., Shelton, R. L., Maciejewski, W., et al. 1999, *ApJ*, 524, 179
- Gaensler, B. M. 1998, *ApJ*, 493, 781
- Guo, Z. & Burrows, D. N. 1997, *ApJL*, 480, L51+
- Hwang, U., Petre, R., & Flanagan, K. A. 2008, *ApJ*, 676, 378
- Jansen, F., Lumb, D., Altieri, B., et al. 2001, *A&A*, 365, L1
- Katsuda, S., Tsunemi, H., Miyata, E., et al. 2008, *PASJ*, 60, 107
- Lazendic, J. S. & Slane, P. O. 2006, *ApJ*, 647, 350
- Leahy, D. & Tian, W. 2005, *A&A*, 440, 929
- Leahy, D. A. 2004, *AJ*, 128, 1478
- Lee, J.-J., Koo, B.-C., Yun, M. S., et al. 2008, *AJ*, 135, 796
- Mewe, R., Gronenschild, E. H. B. M., & van den Oord, G. H. J. 1985, *A&As*, 62, 197
- Miceli, M., Bocchino, F., & Reale, F. 2008, *ApJ*, 676, 1064

- Noriega-Crespo, A., Hines, D. C., Gordon, K., et al. 2008, ArXiv e-prints, 804
- Park, S., Hughes, J. P., Burrows, D. N., et al. 2003a, ApJl, 598, L95
- Park, S., Hughes, J. P., Slane, P. O., et al. 2003b, ApJl, 592, L41
- Petruk, O. 2001, A&A, 371, 267
- Pineault, S., Landecker, T. L., & Routledge, D. 1987, ApJ, 315, 580
- Pineault, S., Pritchett, C. J., Landecker, T. L., Routledge, D., & Vaneldik, J. F. 1985, A&A, 151, 52
- Rho, J. & Borkowski, K. J. 2002, ApJ, 575, 201
- Rho, J. & Petre, R. 1998, ApJl, 503, L167
- Rosado, M., Arias, L., & Ambrocio-Cruz, P. 2007, AJ, 133, 89
- Shelton, R. L., Cox, D. P., Maciejewski, W., et al. 1999, ApJ, 524, 192
- Shelton, R. L., Kuntz, K. D., & Petre, R. 2004, ApJ, 611, 906
- Slane, P., Smith, R. K., Hughes, J. P., & Petre, R. 2002, ApJ, 564, 284
- Snowden, S. & Kuntz, K. 2007, XMM-Newton ESAS manual, <ftp://xmm.esac.esa.int/pub/xmm-esas/xmm-esas.pdf>, 2
- Taylor, A. R., Gibson, S. J., Peracaula, M., et al. 2003, AJ, 125, 3145
- Tilley, D. A., Balsara, D. S., & Howk, J. C. 2006, MNRAS, 371, 1106
- Troja, E., Bocchino, F., Miceli, M., & Reale, F. 2008, A&A, 485, 777
- Troja, E., Bocchino, F., & Reale, F. 2006, ApJ, 649, 258
- White, R. L. & Long, K. S. 1991, ApJ, 373, 543
- Woosley, S. E. & Weaver, T. A. 1995, ApJs, 101, 181